# Seismicity constraints on stress regimes along Sinai subplate boundaries

ALI K. ABDEL-FATTAH[1,2], SAAD M. MOGREN[1] AND SATTAM ALMADANI[1]

1 Department of Geology and Geophysics, College of Science, King Saud University, Riyadh, Saudi Arabia (ali_kamel100@yahoo.co.uk)

2 National Research Institute of Astronomy and Geophysics, Helwan, 11421 Cairo, Egypt

*Received: November 6, 2014; Revised: August 25, 2015; Accepted: September 8, 2015*

## ABSTRACT

*The relative movement between African, Arabian and Eurasian plates has significantly controlled the tectonic process of Sinai subplate region, although its kinematics and precise boundaries are still doubtful. The respective subplate bounded on both sides by the Aqaba-Dead Sea transform fault to the east and the Gulf of Suez, the only defined part, to the west. Seismicity parameters, moment magnitude relation and fault plane solutions were combined to determine the active tectonics along the aforementioned boundaries. Seven shallow seismogenic zones were defined by the heterogeneity in stress field orientations. Along the eastern boundary, the average fault plane solution obtained from the moment tensor summation (MTS) reveals a sinistral strike-slip faulting mechanism. The corresponding seismic strain rate tensor showed that the present tectonic stress producing earthquakes along the boundary is dominated by both NW-SE compression and NE-SW dilatation. Towards the north, the average focal mechanism showed a normal faulting mechanism of N185°E compression and an N94°E extension in the Carmel Fairi seismic zone. On the other hand, the active crustal deformation along the western boundary (Gulf of Suez region) showed a prevailing tensional stress regime of NE to ENE orientations; producing an average fault plane solution of normal faulting mechanism. The seismic strain rate tensor reveals a dominant stress regime of N58°E extension and N145°E compression in consistence with the general tectonic nature in northeastern Africa. Finally, the extensional to strike-slip stress regimes obtained in the present study emphasize that the deformation accommodated along the Sinai subplate boundaries are in consistence with the kinematics models along the plate boundaries representing the northern extremity part of the Red Sea region.*

Keywords: moment tensor summation, focal mechanism, deformation, stress, Sinai subplate

## 1. INTRODUCTION

The Sinai subplate is bounded by the Arabian plate from the east, by the African plate to the west and to the north by the Anatolian plate (*Salamon et al., 2003*). The relative



Stud. Geophys. Geod., 60 (2016), 268–279, DOI: 10.1007/s11200-014-0968-1

tectonic interaction between the aforementioned continental plates and Sinai subplate controls the tectonic process controlling the region. Although kinematics and precise boundaries of Sinai subplate are still doubtful, seismicity demarcate active seismic trends of the Aqaba-Dead Sea Fault System, the Gulf of Suez and the Cyprian Arc (Fig. 1). In the geodynamic model of Sinai subplate, the Aqaba-Dead Sea fault system represents the boundary to the east while the Gulf of Suez is considered the partially defined segment acting the boundary to the west (*Le Beon et al., 2008*). Moreover, no structural or seismic evidence of the western boundary of the subplate is distinguished towards the north (e.g., *Robson, 1971*; *Tapponnier and Armijo, 1985*).

GPS measurements indicated that spreading rate varied from 14 ± 1 mm/year at 15°N to 5.6 ± 1 mm/year along the Red Sea (*McClusky et al., 2003*). Recently, GPS results of *Mahmoud et al. (2005)* showed a left lateral deformation at 1.9 ± 0.3 mm/yr and an extensional deformation at 1.5 ± 0.4 mm/yr along the Gulf of Suez, while a left-lateral deformation at 4.4 ± 0.3 mm/yr was revealed along the Gulf of Aqaba-Dead Sea transform fault. The results of *Reilinger et al. (2006)* revealed N16°W motion of Sinai subplate with respect to Africa at 1.6 ± 1.1 mm/yr. Large-scale GPS data for ten years, as analyzed by *Reilinger et al. (2006)*, showed a slip rate along Wadi Araba at 4.4 ± 0.3 mm/yr. Along Carmel Fault, *Sadeh et al. (2012)* identified rates of 0.7 mm/yr and 0.6 mm/yr for left-lateral and extensional deformations, respectively.

Improved knowledge of Sinai subplate kinematics has a vital importance to clarify the active tectonic processes generating large size earthquakes in the region. A number of studies have been performed to define active crustal deformation using geological, seismological, and GPS data. The seismological aspects are one of particular interest in the region where geologic and geodetic data are not enough to be considered for quantitative analysis; showing the existence of possible faults. In the present study, we aim to constrain stress regimes along the Sinai subplate boundaries using earthquake data to improve our knowledge on orientation and style of deformation. The analysis followed in the present study is based on the moment-tensor summation of well defined focal mechanisms of shallow earthquakes to accurately define the deformation pattern and to distinguish the seismic from aseismic deformation and even to evaluate earthquake hazard in the investigated area. This will emphasize our understanding of active tectonics and recent geodynamics of the Sinai subplate as the area ringed partially by a number of active plate boundaries.

## 2. METHOD OF ANALYSIS AND THE DATA USE

The approach followed in this study complied to the formulations demonstrated by *Kostrov (1974)*. The approach has been widely applied in different tectonic regions (*Jackson and McKenzie, 1988*; *Papazachos et al., 1992*; *Kiratzi, 1993*; *Kiratzi and Papazachos, 1995* and *Papazachos and Kiratzi, 1996*). Herein, the approach is briefly described. The tensor representing average strain rate $\dot{\varepsilon}_{ij}$ is given by:

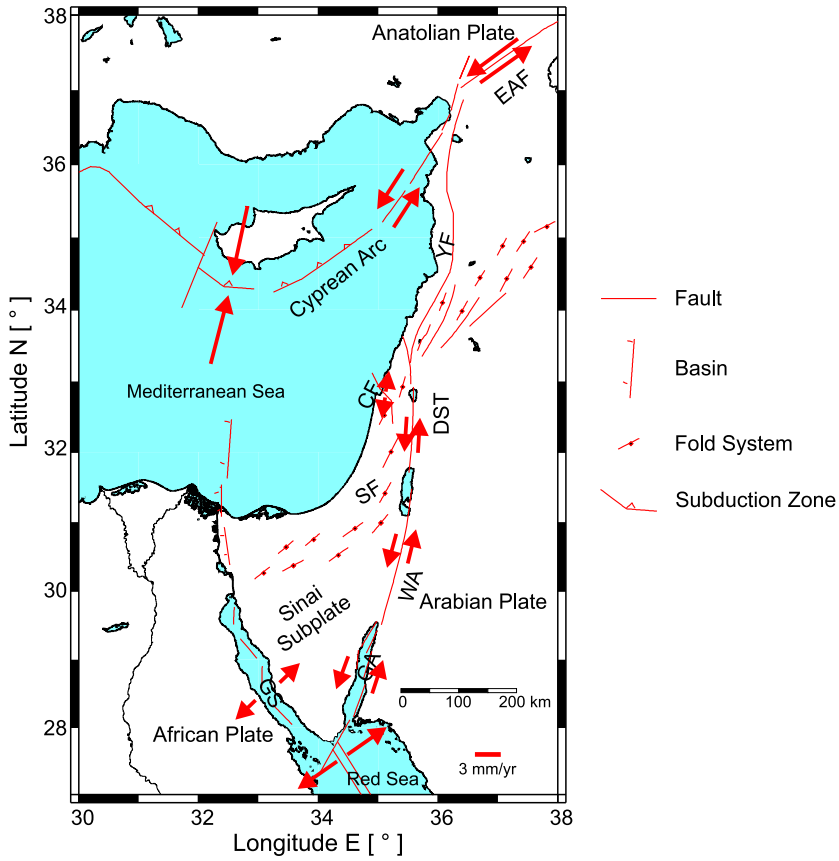


**Fig. 1.** Tectonic map of the eastern Mediterranean region showing plate boundaries and main faults (lines). GS: Gulf of Suez, GA: Gulf of Aqaba, WA: Wadi Araba, DST: Dead Sea Transform, CF: Carmel Fault, YF: Yammouneh Fault, EAF: East Anatolian Fault, SF: Syrian Fold System. Arrows indicate sense of tectonic motion between plates. The length of arrows is proportional to values that characterize the movements along the plate boundaries in the region as determined by *Mahmoud et al. (2005)*.

$$\dot{\varepsilon}_{ij} = \frac{1}{2\mu VT}\sum_{n=1}^{N} M_{n,ij} = \frac{1}{2\mu VT}\dot{M}_o F_{ij} \ , \quad i,j = 1, 2, 3 \ , \tag{1}$$

where $\sum_{n=1}^{N} M_{n,ij}$ is summation of moment tensors over $N$ earthquakes located within a volume $V$ seismically deformed in $T$ years, $\mu$ is the rigidity in the crust ($3 \times 10^{11}$ dyn/cm$^2$), $\dot{M}_o$ is the scalar moment and $F_{ij}$ is a tensor representing the average

of focal mechanism parameters as expressed by *Aki and Richards (1980)*. The moment rate, $\dot{M}_o$, is empirically estimated from *Molnar (1979)* based on the Gutenberg-Richter relation and the relation of moment-magnitude for the study region. To this end, the components of slip rate, $U_{ij}$, are calculated along three dimensional vectors (width, length, and thickness) of dislocation zone using the equations:

$$\begin{aligned} U_{12} &= \frac{1}{2\mu I_3 I_2}\dot{M}_o F_{12}\ , \quad U_{13} = \frac{1}{2\mu I_2 I_3}\dot{M}_o F_{13}\ , \quad U_{23} = \frac{1}{2\mu I_1 I_3}\dot{M}_o F_{23}\ , \\ U_{21} &= \frac{1}{2\mu I_3 I_1}\dot{M}_o F_{21}\ , \quad U_{31} = \frac{1}{2\mu I_2 I_1}\dot{M}_o F_{31}\ , \quad U_{32} = \frac{1}{2\mu I_1 I_2}\dot{M}_o F_{32}\ . \end{aligned} \tag{2}$$

where $I_1$, $I_2$ and $I_3$ are the length, width and thickness of the seismically deformed zone, respectively. It is inevitable to rotate the vector $F_{ij}$ around the reference system of the dislocation zone to be conveniently used in Eqs (1) and (2).

To apply the aforementioned procedure, prior information on the shape and size of a homogeneous seismogenic province is required. Such information can be obtained by integration of geological and seismological data. The moment tensor can be retrieved from focal mechanism parameters, the seismicity parameters of Gutenberg-Richter relationship and the relation of moment-magnitude. A catalogue of earthquakes for the period from 1964 to 2015 was compiled from the publications of the International Seismological Centre (ISC). The focal mechanism solutions data were taken from published works (Abdel-Fattah et al., 1997; *Abou Elenean, 1997*; *Salamon et al., 2003*; *Hofstetter et al., 2007*; *El-Hadidy, 2009* and *Morsy et al., 2011*) in additional to ISC, USGS and Harvard moment tensor solutions. The spatial distribution of epicentres and hypocenters of the earthquake activity in the study area is shown in Fig. 2. The seismicity demarcates the eastward and westward boundaries of Sinai subplate, including the Gulf of Aqaba, Dead Sea fault system, and the Gulf of Suez with a well defined boundary on the Gulf of Aqaba-Dead Sea trend and a partially defined boundary on the other side of the Gulf of Suez region. In additional to geological occurrences, the identification of specific seismic zones is basically defined depending on the nature of spatial distribution of earthquakes and the uniformity of stress field orientations. Taking into consideration the source zones delineated by *Deif et al. (2009)*, the distinct seismic sources are recognized based on the homogeneity in fault plane solutions and in consistence with the major structural and seismotectonic features. The source zones were defined by compiling the distribution of epicenters and hypocenters, structural trends, surface geology, and focal mechanisms. Seven seismic zones have been delimited, as shown in Fig. 2, due to the compilation of priori information such as frequency-magnitude distribution of earthquakes, fault plane solutions, surface geology, and structural settings. The priori information was taken from different sources (*Deif et al., 2009*). The distinct seismic sources are recognized based on the homogeneity in fault plane solutions and their consistency with the major structural and seismotectonic features. The seismogenic zone thickness, $I_3$, is determined on the basis of the distribution of hypocentres as shown in Fig. 2. The average fault plane solution derived from the moment tensor summations for

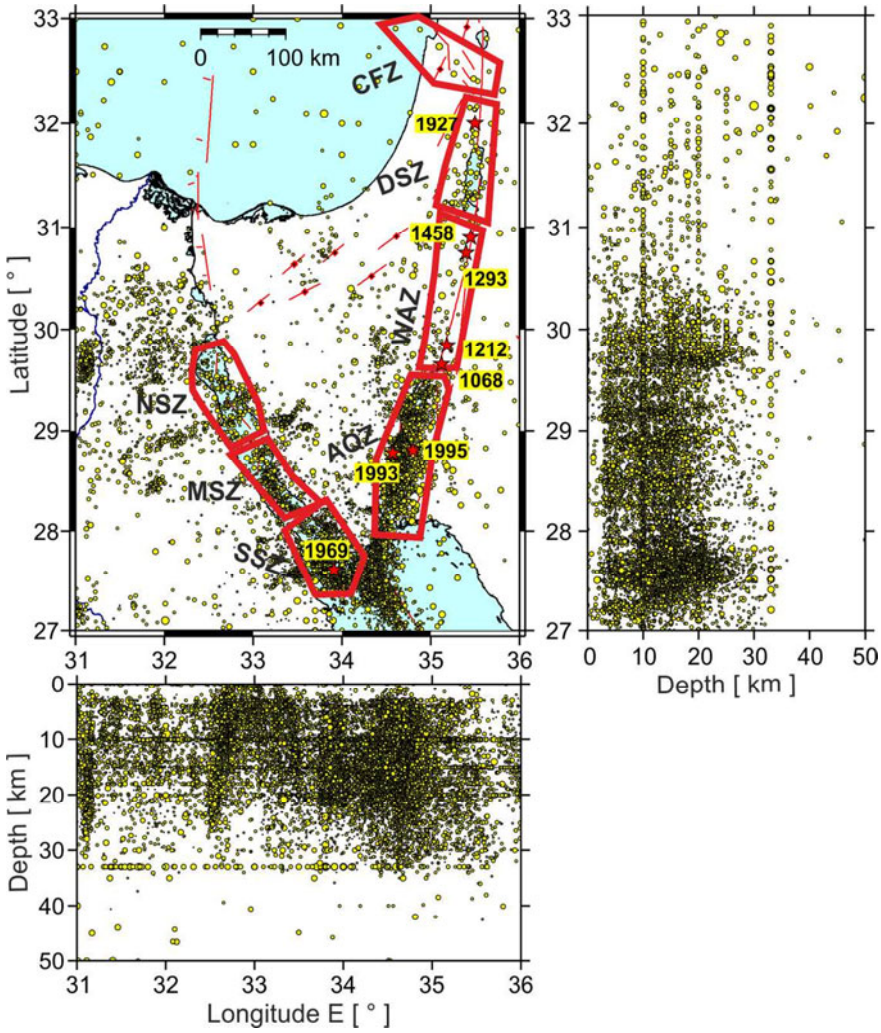


**Fig. 2.** The map shows the epicentral distribution of earthquakes (circles) in the study area from 1900 to 2015. Two vertical cross-sections of hypocenters distribution parallel to the latitude and longitude are also shown. The circle radii are proportional to earthquake magnitudes. The maximum earthquake of $M_w = 7.3$ occurred in Gulf of Aqaba on 22 November 1995. Seven regions of seismic sources have been delimited by polygons, referred to as seismogenic sources in the text. NSZ: North Gulf of Suez Zone, MSZ: Middle Gulf of Suez Zone, SSZ: South Gulf of Suez Zone, AQZ: Gulf of Aqaba Zone, WAZ: Wadi Araba Zone, DSZ: Dead-Sea Zone, CFZ: Carmel Fault Zone. The epicentres (stars and years) of the largest earthquakes ($M > 6$) are also shown.

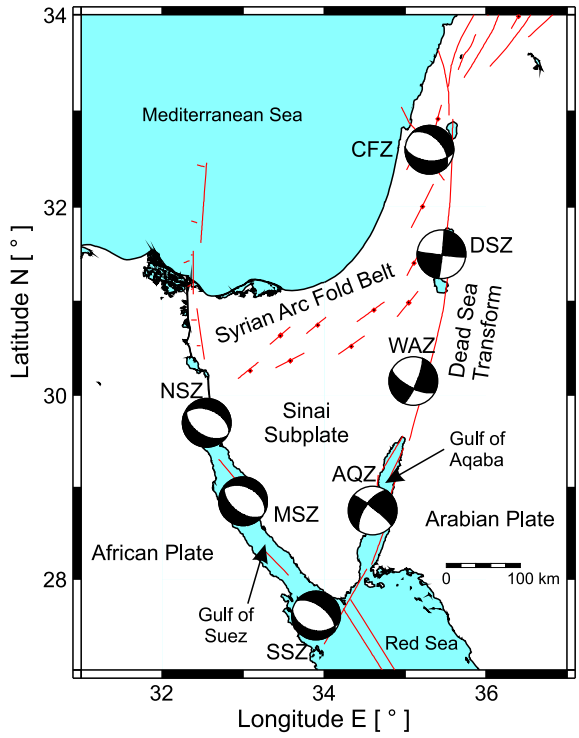


**Fig. 3.** The averaged fault-plane solutions derived from the moment tensor summation (Eq. (1)) for each seismogenic source, shown in Fig. 2. NSZ: North Gulf of Suez Zone, MSZ: Middle Gulf of Suez Zone, SSZ: South Gulf of Suez Zone, AQZ: Gulf of Aqaba Zone, WAZ: Wadi Araba Zone, DSZ: Dead-Sea Zone, CFZ: Carmel Fault Zone.

each seismic zone is shown in Fig. 3. The seismicity parameters of Gutenberg-Richter relation are taken from *Deif et al. (2009)*. For the moment-magnitude relation, the relation derived by *Hofstetter (2003)* for the Gulf of Aqaba is used. The relation is given by

$$\log M_o = (1.5 \pm 0.05) M + (15.4 \pm 0.2), \tag{3}$$

which is consistent with the relation of moment-magnitude $\log M_o = 1.5M + 16.1$ of *Hanks and Kanamori (1979)*, that used for earthquake analysis in the region (*Shapira and Hofstetter, 1993*). Therefore, the relation for the Gulf of Suez region has been used because the digital recording system has been only recently installed and no moment-magnitude relation has been established so far in the region. The priori data required to perform the present analysis are listed in Table S1 (Supplementary Data). To consider the annual moment rate $\dot{M}$ in the calculations, the formulation of *Molnar (1979)* was used

$$\dot{M}_o = \frac{A}{1-B} M_{o,max}^{1-B}, \quad A = 10^{a+(bd/c)}, \quad B = \frac{b}{c}, \tag{4}$$

where $M_{o,max}$ is the scalar moment of the largest observed earthquake, the constants $a$ and $b$ satisfy the Gutenberg-Richter relationship, and the constants $c$ ($1.5 \pm 0.05$) and $d$ ($15.4 \pm 0.2$) fit the relation of moment-magnitude. Using *Molnar's (1979)* formula, the strain rate can be efficiently estimated by incorporating the effects of small and large earthquakes to consider total deformation rate.

## 3. RESULTS: RATE OF ACTIVE CRUSTAL DEFORMATION

The calculations seismic deformation rates were conducted for the defined seven zones, according to the analysis method described above. We estimated the rates of seismic moment release ($\dot{M}_o$) and focal mechanism tensor ($F_{ij}$) for each delineated seismotectonics zone (Fig. 2) along the eastward and westward boundaries of Sinai subplate. Consequently, the strain rate ($\dot{\varepsilon}_{ij}$) and velocity tensor ($U_{ij}$) were estimated. The results obtained from the present analysis for each seismogenic source zone are summarized in Table 1; giving the elements of the strain rate ($\dot{\varepsilon}_{ij}$) and velocity tensor ($U_{ij}$), and its eigenvalues that were derived from the moment tensor summation. Fig. 4 shows the pattern of deformation in terms of velocity rates, divergent and convergent motions along the plat boundaries bounded Sinai subplate.

Along the Gulf of Aqaba seismic zone (AQZ), the six components of the tensor, $F_{ij}$, reflect an average focal mechanism solution with strike of 204°, dip of 62° and slip of –9°, as shown in Fig. 3 and listed in Table 1. The maximum eigenvalue corresponding to dilatation ($T$) is 0.66, while minimum eigenvalue corresponding to compression ($P$) was 0.38. The dimensions of the deformed volume of the Gulf of Aqaba were taken from seismicity distribution in Fig. 2; reflecting 170 km length and 50 km width. The thickness of the seismogenic layer was estimated at 20 km as the recent waveform inversion of the 1995 earthquake revealed that the earthquake occurred at the focal depth lower than 20 km, as estimated by *Klinger et al. (1999)*; *Pinar and Turkelli (1997)* and *Abdel-Fattah et al. (2006)*. The deformation velocities show an ENE-WSW extension of 0.011 mm/yr and a NNW-SSE compression of 0.007 mm/yr in the AQZ.

In the Wadi Araba zone (WAZ), the components of the tensor, $F_{ij}$, yielded an average fault plane solution with strike of 118°, dip of 67° and slip of –166° (Table 1 and Fig. 3). The maximum eigenvalue corresponding to $T$ axis was 0.9, while minimum eigenvalue corresponding to $P$ axis was 0.8; revealing strike-slip faults. Seismic velocity tensor shows that a N150°E compression of 0.19 mm/yr and an N61°E dilatation of 0.13 mm/yr the WAZ dominate in the WAZ.

The average fault plane solution in the Dead Sea zone (DSZ) has a strike of 6°, dip of 88° and rake of –2° as shown in Fig. 3 and listed in Table 1. The maximum eigenvalue corresponding to $T$ axis was 0.61, while minimum eigenvalue corresponding to $P$ axis was 0.41. The depth extent of the seismogenic layer in the DSZ was estimated at 15 km depending on the waveform analysis of *Abou Elenean et al. (2009)*. The zone is seismically deformed by a dilatation of 0.09 mm/yr along N49°E and a compression of 0.08 mm/yr along N139°E.

**Table 1.** Strain-rate and velocity tensors for each seismogenic source.

| Source | Elements of the Strain-Rate Tensor [$10^{-8}$/yr] | | | | | |
|---|---|---|---|---|---|---|
| | $\dot{\varepsilon}_{11}$ | $\dot{\varepsilon}_{12}$ | $\dot{\varepsilon}_{13}$ | $\dot{\varepsilon}_{22}$ | $\dot{\varepsilon}_{23}$ | $\dot{\varepsilon}_{33}$ |
| AQZ | –0.004233 | 0.005892 | 0.002061 | 0.008757 | 0.003491 | –0.004523 |
| WAZ | –0.142133 | 0.142498 | –0.062023 | 0.203204 | 0.062585 | –0.061070 |
| DSZ | –0.003123 | 0.106571 | –0.002182 | 0.045282 | 0.001320 | –0.042159 |
| CFZ | 0.008084 | 0.005555 | –0.001337 | –0.001946 | 0.000300 | –0.006139 |
| SSZ | 0.012436 | 0.006167 | 0.002909 | 0.002480 | 0.005333 | –0.014917 |
| MSZ | 0.002964 | 0.002144 | –0.000505 | 0.000930 | –0.000784 | –0.003894 |
| NSZ | –0.004233 | 0.005892 | 0.002061 | 0.008757 | 0.003491 | –0.004523 |
| | Elements of the Velocity Tensor [mm/yr] | | | | | |
| | $U_{11}$ | $U_{12}$ | $U_{13}$ | $U_{22}$ | $U_{23}$ | $U_{33}$ |
| AQZ | 0.001825 | 0.008689 | 0.000939 | 0.001725 | 0.000773 | –0.000679 |
| WAZ | –0.107878 | 0.135072 | –0.015064 | 0.050419 | 0.021721 | –0.009161 |
| DSZ | –0.004997 | 0.085257 | –0.000655 | 0.018113 | 0.000396 | –0.006324 |
| CFZ | –0.004778 | –0.000619 | 0.000222 | 0.003145 | 0.000346 | –0.000921 |
| SSZ | 0.001912 | 0.005376 | 0.000360 | 0.005700 | –0.001787 | –0.002238 |
| MSZ | 0.000016 | 0.001099 | –0.000023 | 0.001553 | 0.000185 | –0.000389 |
| NSZ | 0.000044 | 0.000144 | –0.000009 | 0.000167 | 0.000009 | –0.000062 |

At Carmel Fairi zone (CFZ), the average focal mechanism solution with strike of 315°, dip of 45° and rake of −60° (Table 1 and Fig. 3) has been derived from the six components of the calculated tensor. The maximum eignevalue corresponding to *T* axis was 0.856, while minimum eignevalue corresponding to *P* axis was 0.763. The seismic velocity rate showed a compression of 0.005 mm/yr along N185°E and an extension of 0.003 mm/yr along N94°E.

In the southern part of the Gulf of Suez zone (SSZ), the average focal mechanism solution with strike of 103°, dip of 37° and rake of −110° (Table 1 and Fig. 3) has been determined from the six components of the calculated tensor. In the middle of the Gulf of Suez zone (MSZ), the average focal mechanism solution is defined by strike of 128°, dip of 51° and rake of −82° (Table 1 and Fig. 3) corresponds to the six components of the calculated tensor. The components of the tensor, $F_{ij}$, yielded an average focal mechanism solution with strike of 123°, dip of 46° and slip of −82° (Table 1 and Fig. 3) in the North Gulf of Suez zone (NSZ). The maximum eignevalues corresponding to *T* axis were 0.373, 0.732, and 0.552 for South, Middle and North of the Gulf of Suez seismic zones, respectively. The deformation velocities show dominant NE-SW extensions of 0.01 mm/yr, 0.002 mm/yr, and 0.003 mm/yr in South, Middle and North of the Gulf of Suez seismic zones, respectively.

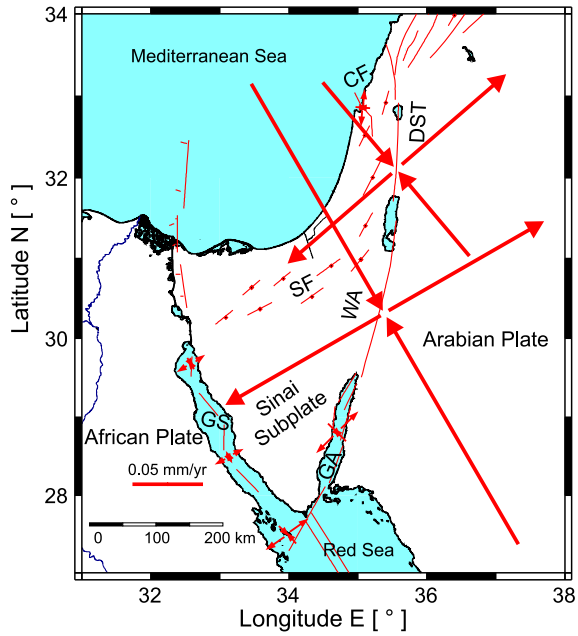


**Fig. 4.** Schematic representation of the stress regimes along the Sinai subplate boundaries. The arrows denote the rate of crustal deformation in mm/yr for each seismogenic source. The length of the arrows is proportional to values that characterize the crustal movements according to the scale. GS: Gulf of Suez, GA: Gulf of Aqaba, WA: Wadi Araba, DST: Dead Sea Transform, CF: Carmel Fault, SF: Syrian Fold System.

## 4. DISCUSSION AND CONCLUSIONS

In the present study the seismic crustal deformation was investigated using moment tensor summation to constrain the stress regime along the Sinai subplate boundaries. The character of the active crustal deformation has been estimated by means of fault plane solutions and the corresponding moment tensors. The averaged fault plane solutions obtained from the moment tensor summation substantiate the tectonic processes acting on the Sinai subplate boundaries. The overall results show that the stress regime along the Sinai subplate boundaries corresponds to extension and shear deformation modes as a result of the relative movements between African, Arabian, and Eurasian plates with respect to the anticlockwise rotation of Sinai subplate. This stress regime is expressed by the existence of normal to strike-slip faults as those that produced earthquakes in the region. This stress regime produced large-sized earthquakes such as the 1927 earthquake of Mb 6.3 that occurred at the northern ultimately of the Dead Sea, the 1969 earthquake of $M_s$ 6.8 that occurred in the Gulf of Suez, Shadwan Island, and the Gulf of Aqaba earthquakes of $M_b$ 6.0 and $M_w$ 7.3 that occurred in 1993 and 1995, respectively. Moreover, the region has

historically experienced large-size earthquakes with recurrence magnitude $M$ 6–7 that could have occurred in the Araba Valley area in 1068 A.D., 1212 A.D., 1293 A.D., and 1458 A.D. as revealed from historical reports and paleoseismological studies (*Abou Karaki, 1987*; *Ambraseys et al., 1994*; *Klinger et al., 2000*). The epicenters of the aforementioned earthquakes are shown in Fig. 2. It is worth mentioned that the calculated rates of seismic deformation are less than that calculated from geological or geodetic observations; indicating that aseismic deformation in the region is much bigger than seismic one.

The boundary bounded the region from the east accommodates the anticlockwise rotation of Sinai subplate with respect to the Arabia plate; corresponding tectonic process of strike-slip motions as suggested by many authors (e.g., *Garfunkel et al., 1981*). In addition, the fault system comprises the regional pull-apart along the eastern boundary generating a local compressional to extensional tectonic process in the zone (*Abu Elenean et al., 2009*). Geological and geophysical evidence revealed that transform and rifting geodynamic processes acted simultaneously on the Gulf of Aqaba-Dead Sea Trend (*Ben-Avraham, 1987*). The transform process started less than 20 Ma B.P., as reported by *Freund et al., 1970*; *Garfunkel, 1981*). The crustal rifting activity propagated northward from the Red Sea into the Aqaba-Dead Sea zone to form a number of pull-apart basins along the zone (*Ben-Avraham, 1985*). The focal mechanisms of the largest event in the zone (the 22nd of November 1995 earthquake of $M_W$ 7.3) exhibited sinistral transform fault mechanism with a small extensional component. The extensional strike-slip deformation is in consistence with the tectonic process of a prevailing tensional stress and left-lateral movement due to the relative motions between the continental plates in the region.

The region of Gulf of Suez exhibited an extensional seismic deformation due to continuation of rifting of the Red Sea. The results reflect a continuation of the horizontal extensional stresses from the south to the north along the Gulf. Our results are compatible with the stress tensor inversion results, as obtained by *Morsy et al. (2011)*; marking extensional stresses of EW orientations are still acting in the middle and northern part of the Suez Gulf.

*Acknowledgements:* The authors would like to extend their sincere appreciation to the Deanship of Scientific Research at King Saud University for funding this Research group NO.(RG-1437-010).The authors thank Dr. Faisal Zaidi for improving the English of the manuscript. Figures were generated using the Genetic Mapping Tool (*Wessel and Smith, 1991*).

Supplementary Data - information on the parameters of the seismogenic source zones of the investigated area can be obtained from
*http://www.ig.cas.cz/sites/default/files/u241/abdel_fattah_2014_0068_tables1_pdf_76651.pdf*

*References*

Abdel-Fattah A.K., Hussein H. and El-Hady S., 2006. Another look at the 1993 Mw = 6.1 and Mw = 7.2 Gulf of Aqaba earthquakes from the analysis of teleseismic waveforms. *Acta Geophys.*, **54**, 260–279.

Abdel-Fattah A.K., Hussein H.M., Ibrahim E.M. and Abu El Atta A.S., 1997. Fault plane solutions of the 1993 and 1995 Gulf of Aqaba earthquakes and their tectonic implications. *Ann. Geofis.*, **XL**, 1555–1564.

Abou Elenean K.M., Mohamed A.M. and Hussein H.M., 2009. Source parameters and ground motion of the Suez-Cairo shear zone earthquakes, Eastern Desert, Egypt. *Nat. Hazards*, **52**, 431–451.

Abou Elenean K.M., 1997. *Seismotectonics of Egypt in Rto the Mediterranean and Red Seas Tectonics*. PhD Thesis. Ain Shams University, Cairo, Egypt.

Abou Karaki, N., 1987. *Synthése et carte sismotectonique des pays de la bordure orientale de la Méditerranée: sismicité du systéme de failles du Jourdain-Mer Morte*. PhD Thesis. University of Strasbourg, Strasbourg, France (in French).

Aki K. and Richards P., 1980. *Quantitative Seismology: Theory and Methods*. Freeman, San Francisco, CA.

Ambraseys N.N., Melville C.P., Adams R.D., 1994. *The Seismicity of Egypt, Arabia and the Red Sea: a Historical Review*. Cambridge University Press, Cambridge, U.K.

Ben Avraham Z., 1985. Structural framework of the Gulf of Elat (Aqaba), northern Red Sea. *J. Geophys. Res.*, **90**, 703–726.

Ben-Avraham Z., 1987. Rift propagation along the southern Dead Sea Rift (Gulf of Elat). *Tectonophysics*, **143**, 193–200.

Deif A., Abou Elenean K., El Hadidy M., Tealeb A. and Mohamed A., 2009. Probabilistic seismic hazard maps for Sinai Peninsula, Egypt. *J. Geophys. Eng.*, **6**, 288–297.

El Hadidy M., 2009. *Seismotectonics and Seismic Hazard Studies for Sinai Peninsula, Egypt*. MSc Thesis. Faculty of Science, Ain Shams University, Cairo, Egypt.

Freund, R., Garfunkel Z., Zak I., Goldberg M. and Weissbrod T., 1970. The shear along the Dead Sea rift. *Philos. Trans. R. Soc. A-Math. Phys. Eng. Sci.*, **267**, 105–127.

Garfunkel Z., 1981. Internal structure of the Dead Sea leaky transform(rift) in relation to plate kinematics. *Tectonophysics*, **80**, 81–108.

Garfunkel Z., Zak Y. and Freund R., 1981. Active faulting in the Dead Sea rift. *Tectonophysics*, **80**, 1–26.

Hanks T.C. and Kanamori H., 1979. A moment magnitude scale. *J. Geophys. Res.*, **84**, 2348–2350.

Hofstetter A., 2003. Seismic observations of the 22/11/2015 Gulf of Aqaba earthquake sequence. *Tectonophysics*, **369**, 21–36.

Hofstetter R., Klinger Y., Amrat A., Rivera L. and Dorbath L., 2007. Stress tensor and focal mechanisms along the Dead Sea fault and related structural elements based on seismological data. *Tectonophysics*, **429**, 165–181.

Jackson J. and McKenzie D., 1988. The relationship between plate motions and seismic moment tensors, and the rates of active deformation in the Mediterranean and Middle East. *Geophys. J. Int.*, **93**, 45–73.

Kiratzi A. and Papazachos C., 1995. Active crustal deformation from the Azores triple junction to Middle East. *Tectonophysics*, **243**, 1–24.

Klinger Y., Rivera L., Haessler H. and Maurin J.-C., 1999. Active faulting in the Gulf of Aqaba: new knowledge from the Mw 7.3 earthquake of 22 November 1995. *Bull. Seismol. Soc. Amer.*, **89**, 1025–1036.

Klinger Y., Avouac J., Abou Karaki N., Dorbath L., Bourles D. and Reyss J., 1974. Slip rate on the Dead Sea Transform fault in northern Araba Valley (Jordan). *Geophys. J. Int.*, **142**, 755–768.

Kostrov B., 1974. Seismic moment and energy of earthquakes, and seismic flow of rock. *Izv. Acad. Sci. USSR Phys. Solid Earth*, **1**, 23–40.

Le Beon M., Klinger Y., Amrat A., Agnon A., Dorbath L., Baer G., Ruegg J., Charade O. and Mayyas O., 2008. Slip rate and locking depth from GPS profiles across the southern Dead Sea Transform. *J. Geophys. Res.*, **113**, B11403, DOI: 10.1029/2007JB005280.

Mahmoud S., Reilinger R., McClusky S., Vernant P. and Tealeb A., 2005. GPS evidence for northward motion of the Sinai block: implications for E. Mediterranean tectonics. *Earth Planet. Sci. Lett.*, **238**, 217–227.

McClusky S., Reilinger R., Mahmoud S., Ben Sari D. and Tealeb A., 2003. GPS constraints on Africa (Nubia) and Arabia plate motions. *Geophys. J. Int.*, **155**, 126–138.

Molnar P., 1979. Earthquake recurrence intervals and plate tectonics. *Bull. Seismol. Soc. Amer.*, **69**, 115–133.

Morsy M., Hussein H., Abou Elenean K. and El-Hady S., 2011. Stress field in the central and northern parts of the Gulf of Suez area, Egypt from earthquake fault plane solutions. *J. Afr. Earth Sci.*, **60**, 293–302.

Papazachos C.B., Kiratzi A. and Papazachos B., 1992. Rates of active crustal deformation in the Aegean and the surrounding area. *J. Geodyn*., **16**, 147–179.

Papazachos C.B. and Kiratzi A., 1996. A detailed study of the active crustal deformation in the Aegean and surrounding area. *Tectonophysics*, **253**, 129–153.

Pinar A. and Turkelli N., 1997. Source inversion of the 1993 and 1995 Gulf of Aqaba earthquakes. *Tectonophysics*, **293**, 279–288.

Reilinger R.E., McClusky S.C., Vernant P., Lawrence S., Ergintav S., Çakmak R., Nadariya M., Hahubia G., Mahmoud S., Sakr K., Arrajehi A., Paradissis D., Al-Aydrus A., Prilepin M., Guseva T., Evren E., Dmitritsa A., Filikov S.V., Gomes F., Al-Ghazzi R. and Karam G., 2006. GPS constraints on continental deformation in the Africa Arabia-Eurasia continental collision zone and implications for the dynamics of plate interactions: *J. Geophys. Res.*, **111**, V05411, DOI: 10.1029/2005JB004051.

Robson D.A., 1971. A detailed magnetic survey of the southern Red Sea. *Geologisches Jahrbuch*, **D13**, 131–153.

Sadeh M., Hamiel Y., Ziv A., Bock Y., Fang P. and Wdowinski S., 2012. Crustal deformation along the Dead Sea Transform and the Carmel Fault inferred from 12 years of GPS measurements. *J. Geophys. Res.*, **117**, B08410, DOI: 10.1029/2012JB009241.

Salamon A., Hofstetter A., Garfunkel Z. and Ron H., 2003. Seismotectonics of the Sinai subplate-the eastern Mediterranean. *Geophys. J. Int.*, **155**, 149–173.

Shapira A. and Hofstetter H., 1993. Source parameters and scaling relationships of earthquakes in Israel. *Tectonophysics*, **217**, 217–226.

Tapponnier P. and Armijo R., 1985. Seismotectonics of northern Egypt. *Terra Cognita*, **5**, 171.

Wessel P. and Smith W., 1991. Free software helps maps and display data. *Eos Trans AGU*, **72**, 441.